Marine productivity estimates from continuous O_2/Ar ratio measurements by membrane inlet mass spectrometry

Jan Kaiser, Matthew K. Reuer, Bruce Barnett, and Michael L. Bender
Department of Geosciences, Princeton University, Princeton, New Jersey, USA

Received 10 May 2005; revised 1 September 2005; accepted 9 September 2005; published 12 October 2005.

[1] Dissolved oxygen/argon (O_2/Ar) ratios in the oceanic mixed layer are indicative of net community production (NCP) because O_2 and Ar share similar physical solubility properties, but only O_2 is biologically produced and consumed. We describe a membrane inlet mass spectrometer (MIMS) that allows continuous high-precision shipboard analysis of O_2/Ar ratios and eventually other gases, calibrated with discrete samples analyzed in the laboratory. We also present O_2/Ar data from the eastern equatorial Pacific. Short-term reproducibilities of 0.05% were achieved. Meridional gradients and small-scale phenomena were clearly resolved. O_2/Ar undersaturations around the equator reflect the interaction of biological and physical forcings. Mixed-layer NCP estimated from wind speed-gas exchange parameterizations was near zero north of 2.75°N, and about 12 mmol m^{-2} d^{-1} south of 6.75°S. Ar supersaturations, calculated from MIMS O_2/Ar measurements and accompanying O_2 concentration measurements, ranged from −0.8 to +3.0%. **Citation:** Kaiser, J., M. K. Reuer, B. Barnett, and M. L. Bender (2005), Marine productivity estimates from continuous O_2/Ar ratio measurements by membrane inlet mass spectrometry, *Geophys. Res. Lett.*, *32*, L19605, doi:10.1029/2005GL023459.

1. Introduction

[2] The dissolved oxygen (O_2) concentration of seawater varies because of fundamental physical and biological processes. These include photosynthesis and respiration, diffusive and bubble-mediated gas exchange, temperature and pressure changes, lateral mixing and vertical diffusion.

[3] The marine oxygen cycle is tightly linked to the carbon cycle via photosynthesis and respiration. In the absence of physical effects, dissolved O_2 constrains the balance of these two biological processes, i.e., net community production (NCP). O_2 can be used as a geochemical tracer that reflects carbon fluxes integrated over characteristic response times. Warming and bubble injection lead to O_2 supersaturation, posing a challenge to this approach.

[4] *Craig and Hayward* [1987] used oxygen/argon (O_2/Ar) ratios to separate O_2 supersaturations into a biological and a physical component. This method is based on the similar solubility characteristics of these two gases with respect to temperature and pressure changes as well as bubble-mediated gas exchange. One can define an O_2/Ar supersaturation, ΔO_2/Ar, as:

$$\Delta O_2/\mathrm{Ar} = \frac{c(O_2)}{c(\mathrm{Ar})} \Big/ \frac{c_{\mathrm{sat}}(O_2)}{c_{\mathrm{sat}}(\mathrm{Ar})} - 1$$

0094-8276/05/2005GL023459

[5] ΔO_2/Ar essentially records the difference between photosynthetic O_2 production and respiration. c is the dissolved gas concentration (in mol m^{-3}) and c_{sat} is the saturation concentration. c_{sat} is a function of temperature, pressure and salinity. This approach, in which discrete samples are collected at sea, stored, and analyzed in the lab, has been widely used in subsequent work [e.g., *Emerson et al.*, 1995; *Hendricks et al.*, 2004; *Spitzer and Jenkins*, 1989].

[6] Here, we describe a new method for continuous underway measurements of O_2/Ar by membrane-inlet mass spectrometry (MIMS), extending earlier oceanographic MIMS applications [*Kana et al.*, 1994; *Tortell*, 2005]. The measured ΔO_2/Ar values can be used in conjunction with suitable wind-speed gas-exchange parameterizations to calculate biologically induced air-sea O_2 fluxes and, where conditions are appropriate, NCP. The inferred NCP values represent rates integrated over the characteristic mixed layer gas exchange times (ratio of mixed layer thickness and piston velocity), typically between 10 and 30 days.

[7] In this paper, we show results of continuous O_2/Ar measurements in the eastern equatorial Pacific (EEP). The equatorial Pacific is a region of considerable interest because of its high-nutrient low chlorophyll character [*Coale et al.*, 1996], its role as oceanic CO_2 source [*Takahashi et al.*, 2002], and its strong coupling of biogeochemical variability to physical forcing. Here, we address a question related to this topic: How does net community production vary in the EEP between the nutrient-poor region north of the equatorial upwelling zone and the nutrient-rich region in the south? We present O_2 and O_2/Ar data in the region between 8°S and 12°N, 110°W and 95°W. The results exemplify the use of MIMS for oceanic productivity studies and its potential to provide large-scale constraints for satellite-based productivity estimates [e.g., *Behrenfeld et al.*, 2005].

2. Methods

[8] Continuous O_2/Ar ratio measurements were made by MIMS on board NOAA R/V Ron Brown during a cruise to service TAO (Tropical Atmosphere Ocean Project) [*McPhaden et al.*, 1998; *McPhaden*, 1995] buoys in the eastern equatorial Pacific in October/November 2003 (RB-03-09-TAO). Meridional and zonal transects were performed in the following order: 12°N to 8°S along 95°W, 95°W to 110°W along 8°S, 8°S to 8°N along 110°W, 110°W to 95°W along 8°N, 8°N to equator along 95°W. The ship's underway sampling system was used to pump water through a Teflon AF membrane (*Random Technologies*) mounted in a stainless steel vacuum manifold, which was

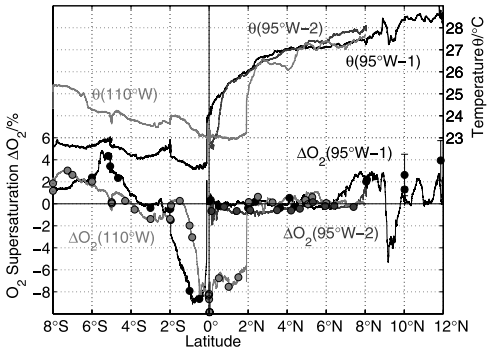

Figure 1. Sea surface temperature (θ) and oxygen supersaturation (ΔO_2) from optode measurements during the three meridional transects of RB-03-09-TAO at 95°W (1: 10/29/03 to 11/05/03; 2: 11/16/03 to 11/18/03, north to south) and 110°W (11/08/03 to 11/14/03, south to north). θ values are plotted as thicker lines than ΔO_2 values. Discrete Winkler O_2 measurements used for calibration of the optode measurements are indicated by filled circles. Error bars are smaller than the symbol size except for the first Winkler measurements between 10°N and 12°N, which were disregarded for the calibration of the optode. See color version of this figure in the HTML.

connected to a quadrupole mass spectrometer (*Pfeiffer Vacuum* Prisma). The intake of the underwater sampling system is located at the bow at a nominal depth of 5 m. The inner diameter of the membrane of 600 μm and the head pressure of the ship's continuous seawater pump (3 bar) determined the volumetric flow rate of 12 cm^3/min through the 10 cm-long membrane tubing. In order to reduce O_2/Ar variations due to temperature and water vapor pressure effects and to avoid degassing, the vacuum manifold with the membrane was held at a constant temperature of 20°C (≥2°C below the surface seawater temperature, SST) and the flight tube was in a thermally insulated box maintained at 40°C.

[9] We calibrated the O_2/Ar ratio measurements with discrete water samples taken from the same seawater outlet as used for the MIMS measurements. 300 cm^3 samples were drawn into pre-evacuated glass flasks poisoned with 7 mg $HgCl_2$ [*Emerson et al.*, 1999]. These samples were later analyzed with an isotope ratio mass spectrometer (IRMS, *Thermo Finnigan*) for their dissolved O_2/Ar ratios and the oxygen triple isotope composition relative to air [*Hendricks et al.*, 2004]. The precision of the IRMS O_2/Ar ratios was about 0.1%, based on analyses of duplicate samples. MIMS O_2/Ar ion current ratio measurements were made every 10 to 30 s and had a short-term stability of 0.05% (standard deviation *s* of 10 sample-mean; error estimates in the following are ±1*s*). The raw O_2/Ar ion current ratios were calibrated by linear regression against the IRMS-measured dissolved O_2/Ar ratios. The mean residual was (0.0 ± 0.3)%.

[10] In addition to the O_2/Ar ratios, O_2 concentrations were measured continuously with an optode (*Aanderaa*), calibrated by automatic Winkler titration of discrete water samples with potentiometric endpoint detection. The analytical precision of the Winkler method was better than 0.1%. Short-term (60 s) precision of the optode measurements was 0.03%. Calibration was achieved by regression of the temperature-corrected optode readings against the Winkler results. The mean difference between calibrated optode and Winkler measurements of the O_2 supersaturation (ΔO_2) was (0.0 ± 0.3)%.

[11] The spatial sampling resolution at a cruise speed of 12 kn is 60–180 m for the MIMS and about 40 m for the optode measurements. Response times (1/*e*-fold) are about 60 s for the MIMS and 30 s for the optode.

[12] Dissolved O_2 was also measured in surface water samples from Niskin bottles in order to assess whether any gas losses occurred from the water pumped from the seawater intake to the laboratory due to warming and potential outgassing or O_2 loss to the pipe walls. A mean ΔO_2 decrease of (0.5 ± 0.3)% was recorded and corrected for in the results presented here. About one third of the ΔO_2 change can be explained with outgassing due to warming by about 0.08°C between seawater intake and outlet in the lab. We did not measure O_2/Ar ratios in Niskin samples on this cruise. On a 2004 cruise of R/V Ka'Imimoana, however, we found that the mean difference between Niskin and continuous measurements was negligible, with a similar change in ΔO_2 as observed for the RB-03-09-TAO cruise. We therefore do not apply any corrections to the ΔO_2/Ar values.

[13] ΔO_2 and ΔO_2/Ar values were calculated from the measured O_2 concentrations, the O_2/Ar ratios, the observed SST and salinities (SSS) from the ship's thermosalinograph and the local barometric pressure. For O_2, the solubility parameterization of *García and Gordon* [1992] based on data from *Benson and Krause* [1984] is used. For Ar, we use the parameterization of *Hamme and Emerson* [2004]. SST measured during the CTD cast was within (0.00 ± 0.04)°C of the temperature at the seawater intake, but SSS had to be corrected upward by 0.20 psu, due to calibration errors of the thermosalinograph. The argon supersaturation (ΔAr) can be inferred from ΔO_2 and ΔO_2/Ar as $\Delta Ar = (\Delta O_2 - \Delta O_2/Ar)/(1 + \Delta O_2/Ar)$.

3. Results

[14] This cruise was the first deployment of our newly-developed instrument. Due to experimental problems with corrosion and clogged membranes, O_2/Ar ratio coverage is not continuous. We obtained reliable O_2/Ar data from the zonal transects and from two partial meridional transects between 8°S and the equator at 110°W and between 8°N and the equator at 95°W.

[15] Continuous ΔO_2 records based on optode data are generally similar between 2°N and 8°N for the 95°W and 110°W transects (Figure 1). Clear differences between 95°W and 110°W are seen in the upwelling region near the equator and smaller differences exist south of the equator, although the ΔO_2 variations at 95°W and 110°W are qualitatively similar between 2°S and 8°S. The surface water ΔO_2 and SST variations reflect the physical transport mechanisms that prevail in the equatorial Pacific. Foremost, the upwelling of cold, O_2-undersaturated waters is evident between the equator and 2°S at 95°W and between just south of 2°N and 1.5°S at 110°W. The northern transition corresponds to the boundary between the westward flowing South Equatorial Current (SEC) and the eastward flowing North Equatorial Countercurrent (NECC). It is particularly

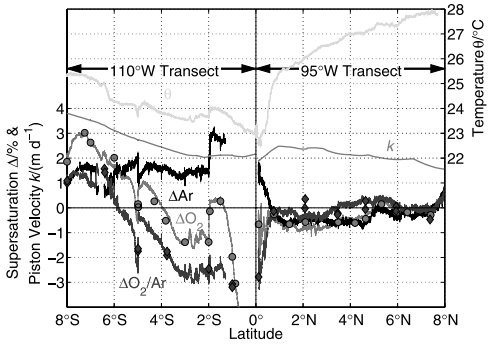

Figure 2. O_2, Ar and O_2/Ar supersaturation (ΔO_2, ΔAr, ΔO_2/Ar), temperature (θ) and piston velocity (k) during the southern part of the 110°W transect and the northern part of the second 95°W transect. Filled circles correspond to Winkler O_2 measurements, filled diamonds to discrete O_2/Ar ratio measurements. See color version of this figure in the HTML.

well-articulated at 2°N near 110°W and occurs within less than half a nautical mile. South of the equator, waters are resaturated at about 2°S at 95°W. However, at 110°W O_2 is again undersaturated between 2°S and 4°S. This could be a remnant due to lateral advection of low O_2 waters from the coastal upwelling region west of Peru [*Toggweiler et al.*, 1991]. Another upwelling region is located between 9°N and 10°N near the boundary between NECC and the westward flowing North Equatorial Current.

[16] Outside of the regions influenced by upwelled waters, O_2 is at or above its saturation concentration, except for a region between 5°N and 1°N sampled during the second 95°W transect. A possible explanation for this undersaturation is to be found in the equally undersaturated Ar concentrations with ΔAr values down to −0.8%. There are two mechanisms that could explain its origin: a recent increase in barometric pressure (which contributed about −0.2%) or a decrease in temperature (which was not observed for the time between the first and second 8°N to 0°-transect at 95°W). Sampling and analysis errors may also contribute. This is suggested by a duplicate discrete ΔO_2/Ar measurement at 2°N, which is 0.5% higher than the ΔO_2/Ar values measured by MIMS. South of the equator, ΔAr values range from 1 to 3% (Figure 2), once again confirming the importance of correcting for the physical supersaturation of O_2.

[17] Figure 2 shows the ΔO_2/Ar data for the northern part of the first 95°W transect and the southern part of the 110°W transect, in addition to ΔO_2 optode measurements, sea surface temperatures and inferred ΔAr values. Both the MIMS and optode give excellent spatiotemporal resolution.

[18] As discussed above, ΔO_2/Ar can be used to estimate the contribution of biology to the observed O_2 supersaturation. Neglecting vertical mixing, a mixed-layer O_2 balance can be written as

$$z_{\mathrm{mix}}\frac{\partial c(\mathrm{O_2})}{\partial t} = G - R - k(\mathrm{O_2})c_{\mathrm{sat}}(\mathrm{O_2})\Delta\mathrm{O_2} + F_{\mathrm{inj}}\chi(\mathrm{O_2}) + F_{\mathrm{exch}}\alpha(\mathrm{O_2})\chi(\mathrm{O_2})/\sqrt{Sc(\mathrm{O_2})}, \quad (1)$$

where z_{mix} is mixed layer depth, G is gross production, R is respiration, $k(O_2)$ is the O_2 gas-exchange coefficient (or piston velocity), $c_{\mathrm{sat}}(O_2)$ is the O_2 saturation concentration, and $F_{\mathrm{inj}}/F_{\mathrm{exch}}$ are air-sea fluxes due to bubble injection and bubble exchange, with the dimensionless parameters being $\chi(O_2)$ – O_2 mixing ratio in air, $Sc(O_2)$ – Schmidt number of O_2, $\alpha(O_2)$ – Ostwald solubility coefficient ([*Hamme and Emerson*, 2002] replace the diffusion coefficient of Hamme and Emerson's equation (4) by the Schmidt number for consistency). Taking the time-derivative of (1) and assuming $\partial^2 c/\partial t^2 = 0$ and constant z_{mix}, G, R, $k(O_2)$, and F_{bubble}, we obtain

$$k(\mathrm{O_2})c_{\mathrm{sat}}(\mathrm{O_2})\Delta\mathrm{O_2} = G - R + F_{\mathrm{inj}}\chi(\mathrm{O_2}) + F_{\mathrm{exch}}\alpha(\mathrm{O_2})\chi(\mathrm{O_2})/\sqrt{Sc(\mathrm{O_2})} - z_{\mathrm{mix}}\sum_i \frac{\partial c_{\mathrm{sat}}(\mathrm{O_2})}{\partial \psi_i}\frac{\partial \psi_i}{\partial t}. \quad (2)$$

ψ represents the influence of temperature, salinity and pressure changes on c_{sat}. A similar equation applies to Ar, with $G = R = 0$. Assuming the same relative response of Ar and O_2 to variations in ψ_i (true to within 1% for seawater) yields $F_{\mathrm{bio}} = G - R =$

$$k(\mathrm{O_2})c_{\mathrm{sat}}(\mathrm{O_2})\left[\Delta\mathrm{O_2} - \frac{k(\mathrm{Ar})}{k(\mathrm{O_2})}\Delta\mathrm{Ar}\right] - F_{\mathrm{inj}}\chi(\mathrm{O_2})\left[1 - \frac{c_{\mathrm{sat}}(\mathrm{O_2})}{c_{\mathrm{sat}}(\mathrm{Ar})}\frac{\chi(\mathrm{Ar})}{\chi(\mathrm{O_2})}\right] - F_{\mathrm{exch}}\alpha(\mathrm{O_2})\chi(\mathrm{O_2})/\sqrt{Sc(\mathrm{O_2})}\left[1 - \sqrt{\frac{Sc(\mathrm{O_2})}{Sc(\mathrm{Ar})}}\right] \quad (3)$$

[19] F_{bio} denotes biologically induced sea-air O_2 fluxes, which can be equated with mixed-layer NCP in areas where the above assumptions are valid and there is negligible vertical mixing across the base of the mixed layer. F_{bio}, G, R, k $c_{\mathrm{sat}}(O_2)$, and F_{bubble} $\chi(O_2)$ are O_2 fluxes in units of mmol m^{-2} d^{-1}. To calculate k, 24 h-average winds at the 10 m-height level (NCEP Reanalysis Project, http://www.cdc.noaa.gov/) are used in combination with the quadratic wind-speed gas-exchange relationship and Schmidt numbers of *Wanninkhof* [1992]. The first bracketed term in (3) is equal to ΔO_2/Ar + (ΔO_2/Ar − 0.01)ΔAr and can be approximated by ΔO_2/Ar. The second/third bracketed terms are about 0.1/−0.01, and will be neglected, because even if the entire observed Ar supersaturation of mostly <2% were due to bubbles, the O_2/Ar supersaturation would be affected by <0.2%. F_{bio} is therefore approximated by $k(O_2)$ $c_{\mathrm{sat}}(O_2)$ ΔO_2/Ar. Values for k are calculated iteratively from the fraction of the mixed layer ventilated on a particular day before sampling, for 120 days backwards in time (M. K. Reuer et al., New estimates of Southern Ocean biological production rates from O_2/Ar ratios and the triple oxygen isotope composition of O_2, submitted to *Deep-Sea Research, Part I*, 2005). Mixed layer depths, taken here as the depth where θ is 0.5°C less than at the surface, vary from 10 m in upwelling regions near the equator at 10°N to 93 m at 2.5°S on the 110°W line. Mixed layer depths only enter implicitly into the calculation.

[20] The derived F_{bio} values are shown in Figures 3 and 4 for the meridional and zonal transects, respectively. Clearly, F_{bio} is higher at 8°S (5–18 mmol m^{-2} d^{-1}) than at 8°N (0–4 mmol m^{-2} d^{-1}). To the extent that F_{bio} can be related to NCP, this meridional gradient is in semi-quantitative agree-

ment with nitrate-based estimates of new production in the eastern equatorial Pacific [*Fiedler et al.*, 1991], which showed about 10 times higher new production at 8°S than at 8°N. This may be due to higher nutrient concentrations in the south, advected into the region by the SEC from the Peru upwelling area, which is supported by modeling results [*Jiang and Chai*, 2005]. Nitrate concentrations were indeed between 6 and 9 mmol m^{-3} south of the equator, and below 0.4 mmol m^{-3} north of 0.5°N at 95°W and north of 2°N at 110°W, suggesting nitrate limitation in the north. Silicate was shown to regulate new production further west in the equatorial Pacific (140°W) [*Dugdale and Wilkerson*, 1998], but was not measured during the present cruise. Low iron concentrations, together with data showing that iron amendments enhance growth [*Gordon et al.*, 1998], indicate that the waters are iron-limited [*Coale et al.*, 1996]. However, iron concentrations seem to be lower south of the equator than north of it, which would rather support a productivity trend opposite to the one we observed [*Jiang and Chai*, 2005].

4. Discussion and Conclusions

[21] Our simple O_2 mass balance approach does not constrain net community production (NCP) where vertical mixing affects the O_2 budget, especially in the equatorial upwelling region. Similar to *Hendricks et al.* [2005] and based on the observed SST and ΔO_2 values, we therefore restrict our analysis to north of 2.75°N and south of 6.75°S. North of the equator, mixed-layer NCP is low throughout a reach of 600 km between 8°N to 2.75°N. South of the equator, we cannot say how far the higher productivities extend north from 6.75°S because of the competing influences of productivity, upwelling/advection of low O_2 waters and gas exchange. Our NCP estimates are similar to previous values derived from discrete O_2/Ar measurements, nitrate budgets and ^{15}N incubations [*Hendricks et al.*, 2005, and references therein].

[22] O_2/Ar ratios, together with wind-speed gas-exchange parameterizations, yield the biologically induced sea-air O_2 flux, F_{bio}. This term integrates NCP over larger reaches of the ocean when vertical mixing and lateral mixing are neglected, but an exhaustive interpretation likely requires an ocean transport model. The potential of MIMS to measure other gases and gas ratios [*Tortell*, 2005] and to provide absolute gas concentrations in connection with precise O_2 concentrations measurements make it a very promising technique, e.g., in order to use of ΔAr values to infer heat fluxes or ΔN_2 values to unravel the influence of bubble injection.

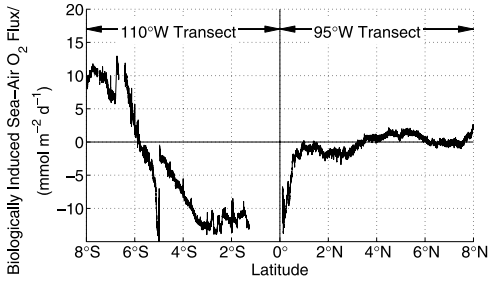

Figure 3. Biologically induced sea-air O_2 fluxes, F_{bio}, inferred from ΔO_2/Ar observations and piston velocities calculated from NCEP 10 m-winds and the wind-speed gas-exchange relationship of *Wanninkhof* [1992].

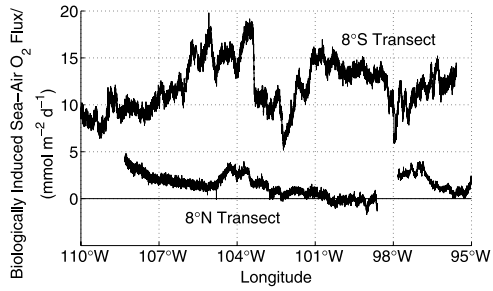

Figure 4. Zonal variations in F_{bio} along the 8°S and 8°N transects.

[23] **Acknowledgment.** We thank the crew and scientific party of NOAA R/V Ron Brown for help and support, the TAO Project (Mike McPhaden and Kristy McTaggart) for providing access and calibrated CTDO results, Greg Cane and Dennis Graham for nitrate measurements and the Gary Comer Foundation, NSF and Princeton University (Hess Fellowships to J. K. and M. K. R.) for funding.

References

Behrenfeld, M. J., et al. (2005), Carbon-based ocean productivity and phytoplankton physiology from space, *Global Biogeochem. Cycles*, *19*, GB1006, doi:10.1029/2004GB002299.

Benson, B. B., and D. Krause (1984), The concentration and isotopic fractionation of oxygen dissolved in fresh water and seawater in equilibrium with the atmosphere, *Limnol. Oceanogr.*, *29*, 620–632.

Coale, K. H., et al. (1996), Control of community growth and export production by upwelled iron in the equatorial Pacific Ocean, *Nature*, *379*, 621–624.

Craig, H., and T. Hayward (1987), Oxygen supersaturation in the ocean: Biological versus physical contributions, *Science*, *235*, 199–202.

Dugdale, R. C., and F. P. Wilkerson (1998), Silicate regulation of new production in the equatorial Pacific upwelling, *Nature*, *391*, 270–273.

Emerson, S., et al. (1995), Chemical tracers of productivity and respiration in the subtropical Pacific Ocean, *J. Geophys. Res.*, *100*, 15,873–15,887.

Emerson, S., et al. (1999), Accurate measurement of O2, N2, and Ar gases in water and the solubility of N2, *Mar. Chem.*, *64*, 337–347.

Fiedler, P. C., et al. (1991), Oceanic upwelling and productivity in the eastern tropical Pacific, *Limnol. Oceanogr.*, *36*, 1834–1850.

García, H. E., and L. I. Gordon (1992), Oxygen solubility in seawater: Better fitting equations, *Limnol. Oceanogr.*, *37*, 1307–1312.

Gordon, R. M., et al. (1998), The behaviour of iron and other trace elements during the IronEx-I and PlumEx experiments in the equatorial Pacific, *Deep Sea Res., Part II*, *45*, 995–1041.

Hamme, R. C., and S. R. Emerson (2002), Mechanisms controlling the global oceanic distribution of the inert gases argon, nitrogen and neon, *Geophys. Res. Lett.*, *29*(23), 2120, doi:10.1029/2002GL015273.

Hamme, R. C., and S. R. Emerson (2004), The solubility of neon, nitrogen and argon in distilled water and seawater, *Deep Sea Res., Part I*, *51*, 1517–1528.

Hendricks, M. B., et al. (2004), Net and gross O_2 production in the Southern Ocean from measurements of biological O_2 saturation and its triple isotope composition, *Deep Sea Res., Part I*, *51*, 1541–1561.

Hendricks, M. B., et al. (2005), The triple oxygen isotope composition of dissolved O_2 in the equatorial Pacific: A tracer of mixing and biological production, *Deep Sea Res., Part I*, in press.

Jiang, M.-S., and F. Chai (2005), Physical and biological controls on the latitudinal asymmetry of surface nutrients and pCO2 in the central and eastern equatorial Pacific, *J. Geophys. Res.*, *110*, C06007, doi:10.1029/2004JC002715.

Kana, T. M., et al. (1994), Membrane inlet mass spectrometer for rapid high-precision determination of N_2, O_2, and Ar in environmental water samples, *Anal. Chem.*, *66*, 4166–4170.

McPhaden, M. J., et al. (1998), The Tropical Ocean-Global Atmosphere observing system: A decade of progress, *J. Geophys. Res.*, *103*(C7), doi:10.1029/97JC02906.

McPhaden, M. J. (1995), The Tropical Atmosphere-Ocean Array is completed, *Bull. Am. Meteorol. Soc.*, *76*, 739–741.

Spitzer, W. S., and W. J. Jenkins (1989), Rates of vertical mixing, gas exchange and new production: Estimates from seasonal gas cycles in the upper ocean near Bermuda, *J. Mar. Res.*, *47*, 169–196.

Takahashi, T., et al. (2002), Global sea-air CO_2 flux based on climatological surface ocean pCO_2, and seasonal biological and temperature effects, *Deep Sea Res., Part II*, *49*, 1601–1622.

Toggweiler, J. R., et al. (1991), The Peru upwelling and the ventilation of the South Pacific thermocline, *J. Geophys. Res.*, *96*, 20,467–20,497.

Tortell, P. D. (2005), Dissolved gas measurements in oceanic waters made by membrane inlet mass spectrometry, *Limnol. Oceanogr. Methods*, *3*, 24–37.

Wanninkhof, R. (1992), Relationship between wind speed and gas exchange over the ocean, *J. Geophys. Res.*, *97*, 7373–7382.

B. Barnett, M. L. Bender, J. Kaiser, and M. K. Reuer, Department of Geosciences, Princeton University, Princeton, NJ 08544, USA. (kaiser@princeton.edu)